CrystEngComm

Accepted Manuscript

ROYAL SOCIETY OF CHEMISTRY

www.rsc.org/crystengcomm

Cite this: DOI: 10.1039/c0xx00000x

www.rsc.org/xxxxxx

ARTICLE TYPE

2-D Lanthanide-organic complexes constructed from 6,7-dihydropyrido(2,3-*d*)pyridazine-5,8-dione: Synthesis, characterization and photoluminescence for sensing small molecules

Waqar Ahmad[a], Lijuan Zhang*[a], Yunshan Zhou*[a]

Received (in XXX, XXX) Xth XXXXXXXXX 20XX, Accepted Xth XXXXXXXXX 20XX
DOI: 10.1039/b000000x

Four isostructural lanthanide-organic complexes $[Ln(HPDH)(ox)(H_2O)]_n$ (Ln = Eu^{3+} **1**, Tb^{3+} **2**, Sm^{3+} **3**, Gd^{3+} **4**; H_2PDH = 6,7-dihydropyrido(2,3-*d*)pyridazine-5,8-dione; H_2ox = oxalic acid) have been synthesized successfully under hydrothermal conditions and characterized by means of elemental analysis, powder XRD, TG-DTA, IR and UV-vis spectroscopy. Complexes **1** and **2** are structurally characterized by single crystal X-ray diffraction analysis. All complexes are composed of 2-D layers, which further construct a 3-D supramolecular network. Each 2-D layer in complexes **1** ~ **4** is composed of 1-D Eu-ox infinite chains, which are further connected by biconnected $HPDH^-$ ligands. The photoluminescent properties of complexes **1** ~ **4** are studied in solid states at room temperature. The singlet energy level (34,722 cm^{-1}) and the lowest triplet energy level (21,786 cm^{-1}) for the ligand H_2PDH are calculated on the basis of its UV-vis absorbance edges (1×10^{-4} M in ethanol) and phosphorescence spectrum of complex **4** at 77 K, respectively. The complexes **1**, **2**, and **3** exhibit metal centered luminescence with characteristic red, green and pink emission, respectively. The energy transfer mechanism and photoluminescence properties are investigated. Complex **1**, in which the energy transition from the triplet energy level ($^3\pi\pi^*$) of ligand $HPDH^-$ to Eu^{3+} cation is more effective, has been selected as a representative to examine the potential for sensing the small molecules by its luminescence properties in different emulsions. EtOH is found to be an excellent enhancing while DMF as highly quenching solvent in this study.

1. Introdution

Photoluminescence based sense ability of lanthanide-organic complexes for the guest molecules has shown extreme potential to be applied in sensing and molecular recognition for many biological processes in living cells and environment,[1,2] because of its obvious merits involved like non consumption of analyte and without using any physical wave-guide for light travel and reference.[3] The scintillating metal-organic coordination polymers remained the promising luminescent probes for small molecules.[4] The key elements to consider in optimizing the performance and efficacy of metal-organic coordination polymers as chemical sensors are sensitivity, selectivity, response time, materials stability and reusability. Recently research has remained focus on understanding the molecular recognition principle of porous metal-organic coordination polymers. In this context, Chen et al[4] pointed out that metals (Eu^{3+} and Tb^{3+}) play a crucial role in molecular recognition by binding interactions of open metal sites with guest molecules, Ma et al[5] suggested that sensing of small molecules are caused by the energy transfer between solvent molecules and ligand, while Jiang et al[6] proposed that pore size of metal-organic coordination polymers has central role in molecular recognitions, and so on. According to literatures, these complexes are mainly thought to perform two functions: first to recognize the guest molecules (receptor) and then show response by luminescence change either by quenching or enhancing (transducer). However, the detailed factors influence the sensing ability of porous lanthanide-organic coordination polymers is still ambiguous. It might be the combinations of different factors as the luminescent properties of metal-organic coordination polymers are very sensitive to and dependent on their structural characteristics, coordination environment of metal, nature of the pore surfaces, and their interactions with guest species through coordination bonds, π···π interactions and hydrogen bonding etc., which have provided the solid grounds to develop luminescent sensing metal-organic coordination polymers.[7]

As compare to 3-D porous lanthanide-organic coordination polymers for sensing guest molecules,[4,5] those possessing 2-D structures have several additional advantages like structural transformations (expansion and contraction),[8] inter-network displacement,[9] slide motion,[10] easy rotation (distortion) of organic linker,[11] inter-network voids[12] and more flexible

porousity.[13] Such properties of 2-D lanthanide-organic coordination polymers allow the diffusion of over sized guest species.[14] However, 2-D lanthanide-organic coordination polymers are rarely investigated for sensing guest molecules.[15]

Taking the advantages of photophysical properties of lanthanide cations, we explored the sensing ability of porous 2-D lanthanide-organic coordination polymers with respect to the nature of guest molecules. A stable and rigid pyridine derivative (6,7-dihydropyrido(2,3-*d*)pyridazine-5,8-dione (H_2PDH)) having conjugation with different coordination atoms (N- and O-) (Scheme 1) is used as ligand for this study. Till now, H_2PDH ligand was only used for constructing Zn^{2+} complex,[16] however lanthanide-organic coordination polymers based on this ligand are not reported till now. In this work, four lanthanide-organic coordination polymers namely $[Ln(HPDH)(ox)(H_2O)]_n$ (Ln = Eu^{3+} **1**, Tb^{3+} **2**, Sm^{3+} **3** and Gd^{3+} **4**) based on H_2PDH and H_2ox (oxalic acid) have been synthesized successfully by hydrothermal method. The energy transfer mechanism and photoluminescence properties of complexes **1** ~ **4** have also been studied. The complex **1** in which the energy transition from the triplet energy level ($^3\pi\pi^*$) of ligand $HPDH^-$ to Eu^{3+} cation is more effective, is selected as a representative to examine the potential for sensing the small molecules, and its luminescent properties in different emulsions of eleven solvents with respect to dielectric constant, coordination ability and normalized Dimroth–Reichardt E_T parameter are also investigated.

Scheme 1 Four isomeric forms of 6,7-dihydropyrido(2, 3-*d*)pyridazine-5,8-dione (H_2PDH).

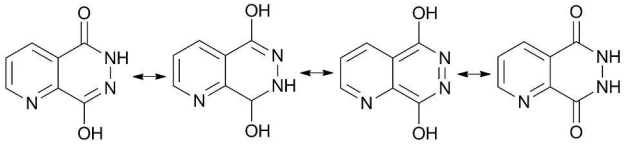

2. Experimental

2.1. Reagents and general techniques

All chemicals are of reagent grade quality, obtained from commercial source without further purification. IR (KBr pellets) spectra were recorded on a Nicolet FT IR-170SX spectrometer in 4000-400 cm^{-1} range. The UV-vis spectra were recorded on Shimadzu UV-2550 spectrophotometer in the range of 200-800 nm. Elemental analyses for C, H, N were performed on a Perkin-Elmer 240C analytical instrument, while analyses for Eu, Tb, Sm, and Gd were performed using an ICPS-7500 model inductively coupled plasma emission spectrometer (ICP-ES) with all samples dissolved in dilute hydrochloric acid. The luminescence decay curve and quantum yield were measured by Edinburgh spectrometer FLS980 by using a tunable laser with wavelength 262.8 nm, bandwidth 10.2 nm, pulse width 930.8 ps and gate 100 ns. Thermogravimetric analyses (TG) and differential thermal analysis (DTA) were performed on a NETZSCH STA 449C unit at a heating rate of 10 $^\circ C \cdot min^{-1}$ under nitrogen atmosphere. Powder X-ray diffraction (XRD) measurements were performed on a Rigaku-Dmax 2500 diffractometer at a scanning rate of $15^\circ/min^{-1}$ in the 2θ range from 5° to 90° with graphite monochromatized Cu Kα radiation (λ = 0.15405 nm). The photo-luminescence spectra were recorded by using a Hitachi F-7000 FL spectrofluorimeter with both excitation and emission slits of 5 nm using a xenon arc lamp as the light source (150w), the photomultiplier tube voltage was 700 V, and the scan speed was 1200 $nm \cdot min^{-1}$.

2.2. Synthesis of ligand 6,7-dihydropyrido(2,3-*d*)pyridazine-5,8-dione (H_2PDH)

The pyridine-2,3-diacidchloride was prepared according to the literature,[17] which was immediately used without further purification. A mixture of pyridine-2,3-diacidchloride 10.2 g (0.05 mol) and hydrazine dihydrochloride 5.25 g (0.05 mol) in aqueous solution of 85% orthophosphoric acid (27 mL) was stirred, then P_2O_5 42.5 g (0.3 mol) was slowly added followed by drop wise addition of $POCl_3$ 15 mL (0.1 mol) (Scheme S1). The progress of the reaction was monitored by thin layer chromatography (TLC) using system MeCN : $CHCl_3$ (4 : 6). The viscous liquid was stirred at 140 °C for 1 h. After cooling, the mixture was poured over crushed ice and put it for 6 h without disturbance, yielding a white solid powder which was washed 3 times (3×5 mL) with distilled water, then dried in air and recrystallized from DMF to get pure white crystalline H_2PDH ligand. Yield: 7.3 g (72.4% based on pyridine-2,3-diacidchloride). Anal. calcd for $C_7H_5N_3O_2$ (H_2PDH): C, 51.53; H, 3.06; N, 25.76; Found: C, 52.04; H, 3.09; N, 25.18; ^{1}HNMR (400 MH_Z, D_2O): δ 9.1 (d, *J* = 4, 1H), δ 8.92 (d, *J* = 8, 1H), δ 8.79 (dd, *J* = 8, 1H), δ 8.17 (dd, *J* = 2, 6, 1H), δ 8.05 (dd, *J* = 4, 8 1H) (Figure S1, Supporting Information). Typical IR bands (KBr, cm^{-1}) (Figure S2): 3194 (s), 3041(s), 2903(s), 1698 (s), 1655 (m), 1608 (m), 1515 (s), 1508 (s), 1473 (m), 1445 (m), 1368 (s), 1278 (s), 1117 (s), 848 (s), 710 (s), 633 (s), 618 (s), 583 (s), 547(s), 490 (s).[18]

2.3. Synthesis of $[Eu(HPDH)(ox)(H_2O)]_n$ 1

The pale yellow needle crystals of complex **1** were obtained by a simple hydrothermal reaction of Eu_2O_3 (0.044 g, 0.12 mmol), H_2PDH (0.081 g, 0.5 mmol) and H_2ox (0.022g, 0.25 mmol) in a 10 mL aqueous solution at 170 °C for 4 days. Yield: 0.0218g (49.7% based on Eu). Anal. calcd. for $C_9H_6N_3O_7Eu$ **1**: C, 25.71, H, 1.43, N, 10.00. Found: C, 25.36, H, 1.21, N, 9.89%. IR (KB, cm^{-1}) (Figure S2): 1641 (s), 1585 (s), 1481(w), 1396 (s), 1217 (s), 1112 (m), 806 (s), 655 (w), 492 (m).

2.4. Synthesis of $[Tb(HPDH)(ox)(H_2O)]_n$ 2

The brown needle crystals of complex **2** were obtained by a similar hydrothermal reaction to that of complex **1** except that Tb_4O_7 (0.046 g, 0.062 mmol) was used instead. Yield: 0.0146 g (31.9 % based on Tb). Anal. calcd. for $C_9H_6N_3O_7Tb$ **2**: C, 25.30, H, 1.40, N, 9.83. Found: C, 25.26, H, 1.21, N, 9.79%. IR (KBr, cm^{-1}) (Figure S2): 1638 (s), 1588 (m), 1482(w), 1358 (s), 1224 (s), 1116 (m), 801 (s), 657 (w), 494 (m).

2.5. Synthesis of $[Sm(HPDH)(ox)(H_2O)]_n$ 3

The light greenish needle crystals of complex **3** were obtained by a simple hydrothermal reaction to that of complex **1** except that Sm_2O_3 (0.043 g, 0.12 mmol) was used instead. Yield: 0.0123g (28.7% based on Sm). Anal. clcd. for $C_9H_6N_3O_7Sm$ **3**: C, 25.83, H, 1.43, N, 10.04. Found: C, 25.55, H, 1.39, N, 10.01%. IR (KBr,

cm^{-1}) (Figure S2): 1643 (s), 1588 (s), 1491(w), 1395 (s), 1216 (s), 1123 (m), 801 (s), 636 (w), 484 (m).

2.6. Synthesis of $[Gd(HPDH)(ox)(H_2O)]_n$ 4

The light brown needle crystals of complex **4** were obtained by a simple hydrothermal reaction to that of complex **1** except that Gd_2O_3 (0.045 g, 0.12 mmol) was used instead. Yield: 0.0130g (29.0% based on Gd). Anal. calcd. for $C_9H_6N_3O_7Gd$ **4**:

Table 1. Summary of crystallographic data for complexes **1** and **2**.

Data	**1**	**2**
Formula	$C_9H_6EuN_3O_7$	$C_9H_6\ TbN_3O_7$
*F*w	420.13	427.09
Crystal system	Triclinic	Triclinic
space group	*P*-1	*P*-1
a (Å)	7.1628(4)	7.1205(3)
b (Å)	7.9091(4)	7.8366(5)
c (Å)	10.2589(4)	10.2949(6)
α (°)	91.372(4)	91.199(5)
β (°)	101.829(4)	107.274(3)
γ (°)	102.587(5)	102.157(4)
V , Å3	553.73(5)	547.33(5)
Z	2	2
ρ_{calcd}, mg/m^3	2.520	2.591
Temp, K	101.8	102.2
F(000)	400	404
μ, mm^{-1}	5.704	6.502
Reflections collected / unique	7234	3624
R(int)	0.0391	0.0420
*R*1, *wR*2 [I > 2ó(I)]	0.0200, 0.0426	0.0305, 0.0672
R1, wR2 (all data)	0.0220, 0.0433	0.0331, 0.0690
GOF	1.043	1.043
Largest diff. peak and hole (e· $Å^{-3}$)	0.704 and -0.655	1.704 and -1.647
CCDC numbers	960628	960630

Table 2. Seleted bond lengths [Å] and angles [°] for complex **1**.

Complex **1**			
Bond lengths			
Eu(1)-O(1)	2.397(20)	Eu(1)-O(6)	2.396(28)
Eu(1)-O(1)# 1	2.383(23)	Eu(1)-O(5)# 3	2.362(24)
Eu(1)-O(4)# 2	2.390(24)	Eu(1)-N(1)# 1	2.604(31)
Bond angles			
O(1)-Eu(1)-O(W7)	153.19(77)	O(3)-Eu(1)-O(6)	148.82(91)
O(3)-Eu(1)-N(1)#1	82.42(83)	O(W7)-Eu(1)-N(1)#1	74.54(81)
O(3)-Eu(1)-O(1)#1	82.50(91)	O(W7)-Eu(1)-O(1)#1	134.06(84)
O(1)#1-Eu(1)-O(1)	66.92 (80)	O(W7)-Eu(1)-O(6)	75.39(85)
O(1)-Eu(1)-O(3)	80.03(87)	O(W7)-Eu(1)-O(5)#3	81.25(80)
O(1)-Eu(1)-O(4)#2	96.01(76)	O(W7)-Eu(1)-O(4)#2	71.88(8)
O(1)-Eu(1)-O(6)	103.41(79)	O(6)-Eu(1)-O(5)#3	68.60(83)
O(1)-Eu(1)-O(5)#3	73.70(73)	O(6)-Eu(1)-O(4)#2	140.27(83)
O(1)-Eu(1)-O(W7)	153.19(77)	O(6)-Eu(1)-O(1)#1	71.02(80)
O(1)-Eu(1)-N(1)#1	131.26(82)	O(6)-Eu(1)-N(1)#1	72.04(83)

Symmetry transformations used to generate equivalent atoms for complex **1**: #1 = 1-x, 2-y, 2-z, #2 = 1-x, 1-y, 2-z, #3 = -x, 2-y, 2-z.

C, 25.41, H, 1.41, N, 9.90. Found: C, 25.13, H, 1.11, N, 9.04%. IR (KBr, cm^{-1}) (Figure S2): 1639 (s), 1584 (s), 1489(w), 1392 (s), 1213(s), 1121 (m), 805 (s), 633(w), 517 (m).

2.8. X-ray Crystallography

Single-crystal X-ray diffraction data were collected on a Bruker APEX2 X-Diffraction Instrument with Mo Kα radiation (λ = 0.71073Å) in the ω scans mode. The structures were solved by direct methods and refined anisotropically using full-matrix least-squares methods with the SHELX 97 program package.[19] The non-hydrogen atoms were located in successive difference Fourier syntheses. The final refinement was performed by full matrix least squares methods with anisotropic thermal parameters for non-hydrogen atoms on F^2.[20] A summary of the crystallographic data and structural determination parameters of complexes **1** and **2** are given in Table 1. CIF files for the structures reported in this paper have been deposited with the Cambridge Crystallographic Data Centre (CCDC). The deposition numbers are given in Table 1. Seleted bond lengths and bond angles for complex **1** is given in Table 2.

3. Results and Discussion

3.1. Discussion on the Synthesis

The pyridine-2, 3-diacidchloride was prepared according to the literature,[17] except that less toxic toluene was used at the place of benzene, as a result the reaction took one hour extra than reported method, and the yield (71% based on pyridine-2,3-dicarboxylic acid) was almost same. The synthesis of H_2PDH ligand has been carried out in one port, quick and easier fashion by stirring

pyridine-2,3-diacidchloride with hydrazine dihydrochloride (1:1) in orthophosphoric acid, followed by slow addition of P_2O_5 and $POCl_3$. Orthophosphoric acid was used for acidic medium, while P_2O_5 and $POCl_3$ were used for ring closure. A satisfactory yield (72.4 %) of H_2PDH ligand is obtained as compared to reported method.[21] The reactions between lanthanide oxides, H_2PDH ligand and oxalic acid (H_2ox) under hydrothermal condition resulted in the formation of four new lanthanide-organic coordination polymers **1** ~ **4**. Under the defined optimal conditions (the molar ratio of $Ln^{3+}/H_2PDH/H_2ox$ = 1:2:1, reaction temperature = 170 °C, reaction time = 4 days), reasonable yield for all complexes was obtained.

3.2. IR Spectra of H_2PDH and Complexes 1 ~ 4

The IR spectrum of free ligand H_2PDH shows strong absorption band at 1698 cm^{-1}, which is assigned to the stretching vibration of the carbonyl group υ(C=O).[22] The medium intensity bands appearing at 1508, 1473, 1445 cm^{-1} can be assigned to the aromatic υ(C=N)/υ(C=C) stretching vibrations of pyridyl ring[23, 24] and the peaks at 3041, 848 and 710 cm^{-1} are assigned to the aromatic C-H bonds. The IR spectra of all complexes **1** ~ **4** are almost similar, the characteristic frequency of the free ligand υ(C=O) at 1698 cm^{-1} shifted toward the lower wave numbers of 1641, 1638, 1643 and 1639 cm^{-1} for complexes **1** ~ **4**, respectively, indicating that the oxygen atom from carbonyl group is involved in coordination interaction with Ln^{3+} in the four complexes.

3.3. Powder XRD

The experimental powder X-ray diffraction patterns of complex **1** (Figure S3(a)), complex **2** (Figure S3(b)), complex **3** (Figure S3(c)) and complex **4** (Figure S3(d)) are almost consistent with the simulated XRD pattern (Figure S3(simulated)) generated on the basis of single crystal X-ray diffraction structural data of complex **1**. The powder XRD patterns of complexes **1** ~ **4** show that they are isomorphous, which is consistent with the single crystal X-ray diffraction analysis described below. The extremely small amorphous signals in the region of 2θ = 5 - 16° imply presence of very little impurity in the resulting bulk product for all complexes **1** ~ **4**.

3.4. Structural Description of [Eu(PDH)(ox)(H_2O)] 1

Single crystal X-ray diffraction analysis reveals that complex **1** and complex **2** are isostructural, thus only the structure of complex **1** will be discussed in detail here as a representation. Complex **1** possesses a two-dimensional (2D) layer network; it crystallizes in triclinic space group *P*-1.

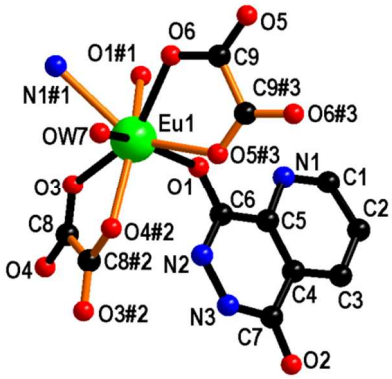

Figure 1 The coordination environment around Eu^{3+} in complex **1** with labeling scheme, atoms composing the asymmetric unit are connected by black-filled bonds, all hydrogen atoms are omitted for clarity. Symmetry codes follow: #1 = 1-x, 2-y, 2-z, #2 = 1-x, 1-y, 2-z, #3 = -x, 2-y, 2-z.

The asymmetric unit of complex **1** contains one Eu^{3+} atom, one $HPDH^-$ ligand, two halves of ox^{2-} ligands and one coordinated water molecule (OW7) (Figure 1).The eight coordinated Eu^{3+} cation is surrounded by two acylamino oxygen atoms (O1 and O1#1) from two different $HPDH^-$ ligands, one pyridyl nitrogen atom (N1#1) from one $HPDH^-$ ligand, four oxygen atoms (O3, O4#2, O5#3 and O6#3) from two different ox^{2-} ligands together with one coordinated water molecule (OW7) (Figure 1). The two Eu1-$O_{hydroxylimino}$ distances (Eu1-O1 = 2.397(20) Å, and Eu1-O1#1 = 2.383(23) Å) and four Eu1-$O_{Oxalate}$ distances (Eu1-O3 = 2.407(30) Å, Eu1-O4#2 = 2.390(24) Å, Eu1-O6 = 2.396(28) Å and Eu1-O5#3 = 2.362(24) Å) are comparable with each other. The Eu1-$N_{pyridyl}$ distance is (Eu1-N1#1 = 2.604(31) Å). Eu1-O_{water} distance (Eu1-OW7 = 2.457 (23) Å) is the longest among all Eu1-O bonds. The O-Eu(1)-O and O-Eu(1)-N bond angles vary from 66.92º to 153.19º and 72.04º to 131.26º respectively in the complex **1** (Table 2).

Each $HPDH^-$ ligand adopts a biconnected coordination mode in complex **1** where its pyridyl N atom and acylamino O atom coordinate to two Eu^{3+} centers in a fashion as shown in Scheme 2, while each oxalate (ox^{2-}) adopts a bidentate coordination mode linking two Eu^{3+} centers.

Scheme 2 Schematic representation of the coordination modes of $HPDH^-$ and ox^{2-} ligands.

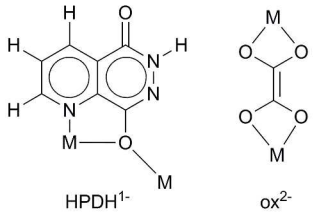

The oxalate anions (ox^{2-}) adopting bi-connected coordination mode are classified into two groups (one group is crystallographically independent of the other group) in view of their orientation. Linkage of the adjacent Eu^{3+} centers by such two groups of ox^{2-} results in the formation of a 1D Eu-ox infinite chain (Figure 2a). The distances between the adjacent Eu^{3+}

centers within 1-D Eu-ox infinite chain, are ca. 6.15 Å and 6.17 Å which depend on the group of ox. The dihedral angle between the adjacent oxalates is 43.70(7)º (Figure 2a).

The 1-D infinite chains are then interconnected by $HPDH^-$ ligands to form a 2-D network. In the 2-D network, the distance between the two adjacent chains is ca. 3.99 Å based on the distance of Eu···Eu (Figure 2b). Within the 2-D network, four $HPDH^-$ ligands and four ox^{2-} ligands linked six Eu^{3+} centers to form a 20-membered $M_6(HPDH)_4(ox)_4$ hexagonal macro circle (size: 3.99 × 6.15 × 6.17 Å based on Eu···Eu distance). The adjacent 2-D layers then link each other by hydrogen bonding and π···π stacking interaction to form 3-D supramolecular framework of complex **1** (Figure 2d). The interlayer π···π stacking interaction (3.626 Å between ring (N1, C1, C2, C3, C4 and C5) of one layer and ring (N2, N3, C4, C5, C6 and C7) of its neighbouring layer is shown as enlargement in Figure 2e. The distance of hydrogen bonding is 2.839 Å (O4···OW7) (Figure S4).

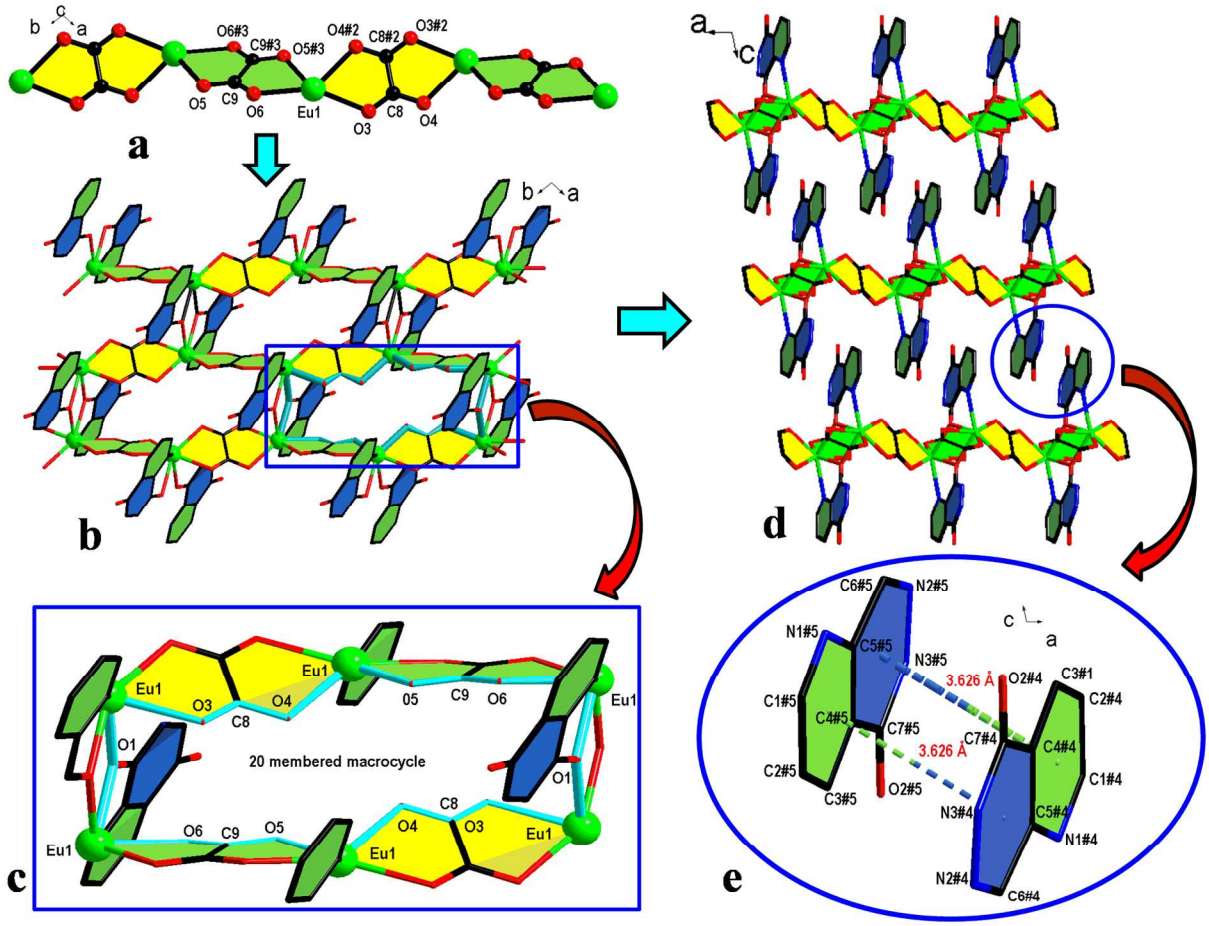

Figure 2 The schematic representation for the formation of 3D supramolecular network: (a) single 1D infinite (-Eu-ox-) chain of complex **1** with partial labeling, where the two groups of ox^{2-} ligands with different orientations are highlighted in green and yellow colors. (b) The 2D layer structure of complex **1** composed of 1D infinite Eu-ox chains linked by $HPDH^-$ ligands. (c) The enhanced sketch of a blue colored rectangle showing a 20 membered macrocycle ($M_6(PDH)_4(ox)_4$) with labeling scheme. (d) The 3D supramolecular framework composed of the 2D layers. (e) The enhanced sketch of a blue colored circle showing the π···π interactions (the broken lines) between the neighboring rings from adjacent 2D layers, the blue fill color of ring shows pyradazine, while light green color shows pyridine ring. All hydrogen atoms and coordinated water molecules (OW7) are omitted for clarity, Color code: Eu, green; O, red; C, black; N, blue. Symmetry code: #2 = 1-x, 1-y, 2-z, #3 = -x, 2-y, 2-z, #4 = 1+x, -1+y, 2-z, #5 = 2-x, 1-y, 2-z.

3.6. Photoluminescent Properties

According to the luminescence principle of lanthanide complexes with organic ligands[25] and the results of Sato et al.,[26] the efficiency of intramolecular energy transfer from organic ligands to the Ln^{3+} is the most key influencing factor for the luminescence properties of lanthanide complexes. The intramolecular energy transfer efficiency depends mainly on the following two energy transfer processes:[27] (1) The energy transfer from the lowest triplet energy ($^3\pi\pi^*$) level of organic ligand to the resonant energy level of Ln^{3+} by Dexter's resonant exchange interaction,[28] (2) the inverse energy transfer from Ln^{3+} to organic ligand by a thermal deactivation mechanism. The triplet energy levels ($^3\pi\pi^*$) of ligands should lie close to the resonant energy levels of the lanthanide cation but sufficiently high to avoid the inverse energy-transfer.[29] According to Reinhoudt's empirical rule,[30] the intersystem crossing process becomes effective only when the energy gap ($\Delta E = {}^1\pi\pi^* - {}^3\pi\pi^*$) between singlet ($^1\pi\pi^*$) and triplet ($^3\pi\pi^*$) energy levels of the ligand is over to the least value of 5000 cm^{-1}.

To explicate the energy transfer processes of the lanthanide coordination complexes, the energy levels of the relevant electronic states of the ligand have been investigated. The singlet

energy level (^{1}s, 34, 722 cm^{-1} (288 nm)) of H_2PDH ligand was estimated by referencing its absorbance edge, which was determined from UV spectrum of H_2PDH (Figure S5). The triplet energy level ($^3\pi\pi^*$) of H_2PDH ligand was found to be 21,786 cm^{-1} (459 nm) based on the phosphorescence spectrum (Figure S6) of the complex Gd(PDH)(ox)(H_2O) **4**.[31] Since the lowest excited state $^6P_{7/2}$ of Gd^{3+} ion is too high to accept energy from ligand, the data obtained from the phosphorescence spectrum of the complex **4** actually reveals the triplet energy level ($^3\pi\pi^*$) of the corresponding ligand.[32] The energy gap ΔE ($^1\pi\pi^*$ - $^3\pi\pi^*$) was calculated to be 12,936 cm^{-1} for H_2PDH ligand, indicating that the intersystem crossing process is effective in all complexes **1** ~ **4** (Figure 3).[33]

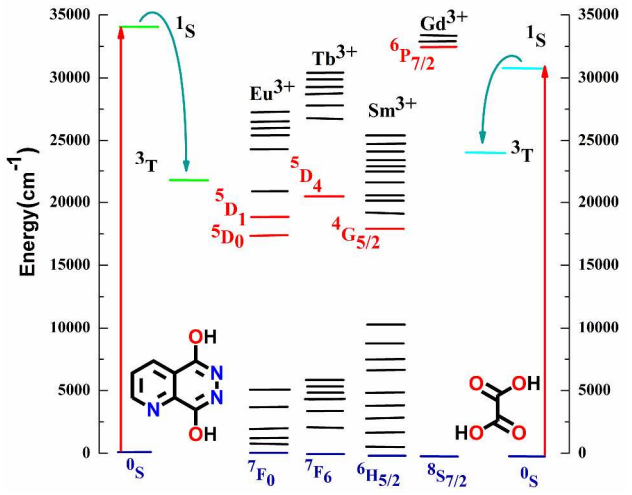

Figure 3 Partial energy diagrams (Jablonski, Tailbones) for the Ln^{3+} ions (Ln = Eu, Tb, Sm and Gd). The main luminescent levels of Ln^{3+} ions are drawn in red, while the fundamental levels are indicated in blue, singlet and triplet energy levels of H_2PDH and H_2ox ligands in green and magenta colors respectively.

Energy gaps between the triplet energy level ($^3\pi\pi^*$) of the corresponding ligands (21,786 cm^{-1} for H_2PDH and 23,753 cm^{-1} for oxalic acid[34]) and the excited resonance energy levels $^5D_1$ of Eu^{3+} (19,000 cm^{-1}), $^5D_4$ of Tb^{3+} (20,500 cm^{-1}), and $^4G_{5/2}$ of Sm^{3+} (17,900 cm^{-1}) are shown in Table 3. Latva's empirical rule[35] explains that an optimal ligand-to-metal energy transfer process for Eu^{3+} needs 2500 < $\Delta E(^3\pi\pi^*$-$^5D_1)$ < 4000 cm^{-1}, and for Tb^{3+} requires 2500 < $\Delta E(^3\pi\pi^*$-$^5D_4)$ <4500 cm^{-1}.

Table 3 Energy gaps (cm^{-1}) between the triplet states ($^3\pi\pi^*$) of H_2PDH and the resonating energy levels of $^5D_1$ (Eu), $^5D_4$ (Tb), $^4G_{5/2}$ and (Sm).

Triplet energy state	$\Delta E(^3\pi\pi^*$ - $^5D_1)$	$\Delta E(^3\pi\pi^*$ - $^5D_4)$	$\Delta E(^3\pi\pi^*$ - $^4G_{5/2})$
$^3\pi\pi^*$ (H_2PDH)	2786	1286	3886
$^3\pi\pi^*$ (H_2ox)	4753	3253	5853

The results in Table 3 show that the energy gap between triplet state ($^3\pi\pi^*$) of H_2PDH ligand and resonating energy level ($^5D_1$) of Eu^{3+} is 2786 cm^{-1}, indicating that the energy transition from the triplet energy level ($^3\pi\pi^*$) of H_2PDH to Eu^{3+} cation is effective. The energy gaps between the triplet level ($^3\pi\pi^*$) of H_2PDH ligand and resonating energy levels ($^5D_4$) of Tb^{3+}, and of $^4G_{5/2}$ of Sm^{3+} $^4F_{9/2}$ are 1286 cm^{-1} and 3886 cm^{-1} respectively, which are not ideal situation for Tb^{3+} and Sm^{3+} luminescence. While the energy gaps between the triplet energy level of H_2ox ligand and $^5D_4$ state of Tb^{3+} are 3253 cm^{-1} respectively, implying that H_2ox is most suitable sensitizer for Tb^{3+} as compare to H_2PDH ligand in this study.[36] This supports the observation of the characteristic emissions of central Eu^{3+}, Tb^{3+} and Sm^{3+} ions in the emission spectra of the complexes and we may deduce that the triplet state energy level of H_2PDH ligand matches better to the resonance energy levels of Eu^{3+} than Tb^{3+}, and Sm^{3+} ions, while oxalic acid ligand matches better with Tb^{3+} than Eu^{3+} and Sm^{3+}.

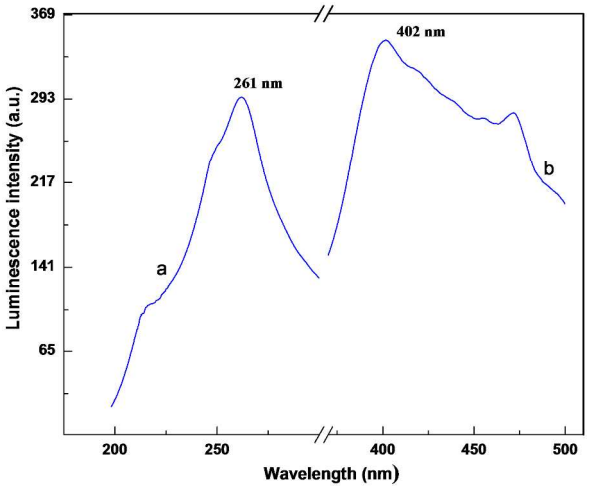

Figure 4 The solid-state excitation (a) and emission spectra (b) of H_2PDH ligand at room temperature.

The photoluminescence properties of the free ligand and complexes **1** ~ **4** were investigated at room temperature. Free H_2PDH ligand displays a photoluminescent emission at 402 nm upon excitation at 261 nm (Figure 4). The main chromospheres of this ligand are the aromatic pyridine and acylamino rings. Complexes **1** and **2** show 8% red shift (maximum band at 282 nm) and complex **3** shows 3% blue shift (maximum band at 253 nm) in the excitation spectra compared with the free ligand (maximum band at 261 nm), respectively.[37] Complex **1** emits characteristic red luminescence from Eu^{3+} ion in the solid state under UV light irradiation, and corresponding excitation and emission spectra of complex **1** are shown in Figure 5.

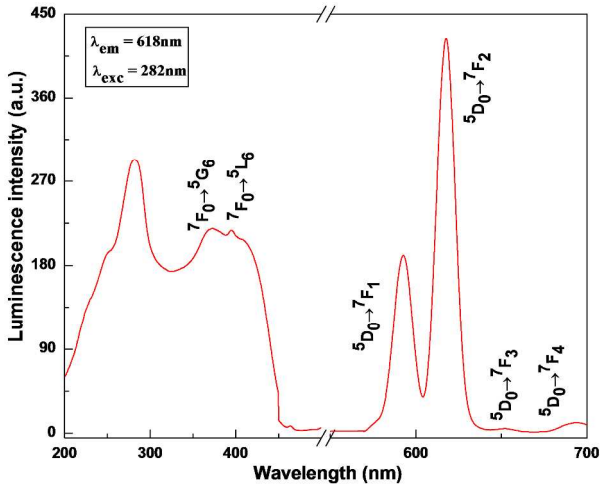

Figure 5 Excitation and emission spectra of [Eu(PDH)(ox)(H_2O)] **1** at λ_{em} = 618 nm and λ_{exc} = 282 nm, respectively.

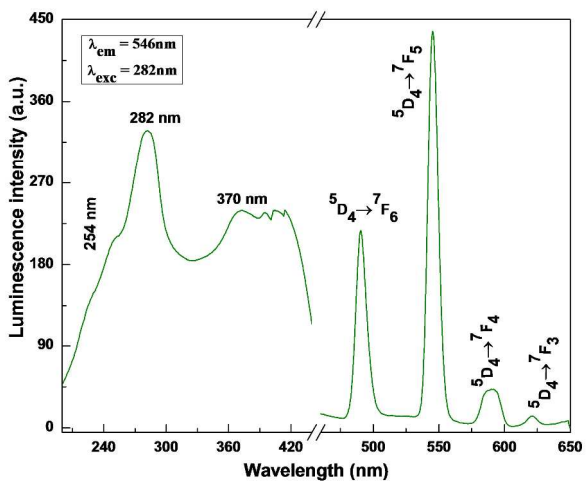

Figure 6 Excitation and emission spectra of [Tb(PDH)(ox)(H_2O)] **2** at λ_{em} = 546 nm and λ_{exc} = 282 nm respectively.

The excitation spectrum of complex **1** reveals a strong broad centered band at 282 nm, which can be ascribed to the electronic transitions of H_2PDH ligand. The peaks at 371 and 395 nm can be assigned to the $^7F_0 \rightarrow {}^5G_6$ and $^7F_0 \rightarrow {}^5L_6$ transitions of Eu^{3+} cation respectively.[38] The detection of band (centered at 282nm) together with its higher intensity relative to the intra-$4f^n$ transitions, points out a more efficient luminescence sensitization via the ligand excited states than the direct intra-$4f^n$ excitation.[39] The emission spectra of complex **1** in solid state at excitation wavelength of 282 nm, shows the sensitized luminescence bands that correspond to the typical Eu^{3+}cation, $^5D_0 \rightarrow {}^7F_n$ (n= 1, 2, 3, 4) transitions (Figure 5).

Complex **1** shows intense red luminescence and strong intensities of magnetic dipole emission at 593 nm and hypersensitive induced electric dipole emission at 617 nm, which are attributed to $^5D_0 \rightarrow {}^7F_1$ and $^5D_0 \rightarrow {}^7F_2$ transition, respectively.[40] The magnetic dipole emission of $^5D_0 \rightarrow {}^7F_1$ transition is relatively weaker and largely independent of the coordination sphere, i.e. the ligand field.[41] The electric dipole $^5D_0 \rightarrow {}^7F_2$ transition centered at 617 nm is extremely sensitive to the symmetry of the coordination sphere of Eu^{3+}.[42] Kirby and Richardson established that the relative intensity of the $^5D_0 \rightarrow {}^7F_2$ and the $^5D_0 \rightarrow {}^7F_1$ emission is a good measure of the symmetry of the first coordination sphere.[43]

The distortion of the symmetry around the metal cation causes an intensity enhancement of electric dipole transitions such as the hypersensitive $^5D_0 \rightarrow {}^7F_2$ transition (Figure 5). The intensity ratio of $^5D_0 \rightarrow {}^7F_2$ / $^5D_0 \rightarrow {}^7F_1$ is 2.23, indicating that Eu^{3+} cation has an asymmetric coordination sphere,[44] as observed in the single crystal structure. Two emission peaks with weak intensities of induced electric dipole emissions at 652 nm and 698 nm correspond to the $^5D_0 \rightarrow {}^7F_3$ and $^5D_0 \rightarrow {}^7F_4$ transitions respectively.[45]

The luminescence of complex **2** was characterized by the emission from the $^5D_4$ state resulting in green luminescence. The room temperature excitation bands of complex **2** under excitaion wavelength of 546 nm posses three main peaks at 254, 282 and 370 nm and few detected small bands between 300 to 450 nm corresponding to intra-configurational forbidden $4f^8 \rightarrow 4f^8$ transition of Tb^{3+} ion.[46] The appearance of a broad band at 282 nm together with its higher intensity relatively to the intra-$4f^8$ transition show an effective luminescence sensitization *via* the ligand's excited states than the direct intra-$4f^8$ excitation[40] (Figure 6).

The emission spectra of complex **2** emits bright green light and exhibits the characteristic transition of $^5D_4 \rightarrow {}^7F_n$ (n = 3, 4, 5, 6) of Tb^{3+} cation under the excitation wavelength of 282 nm of UV light. The medium intensity emission band at 491 nm is ascribe to $^5D_4 \rightarrow {}^7F_6$ transition of Tb^{3+} cation and a sharp intense line emission band at 546 nm corresponding to $^5D_4 \rightarrow {}^7F_5$ of Tb^{3+} ion are observed, which give intense green luminescence, while the two weak emission bands at 587 nm and 620 nm may attributed to $^5D_4 \rightarrow {}^7F_4$ and $^5D_4 \rightarrow {}^7F_3$ transitions respectively.[47]

The excitation bands for complex **3** under the emission wavelength of 561 nm show three main peaks at 224, 253 and 278 nm. There are also some small bands at 363 and 377 nm which are corresponding to $^4D_{3/2} \leftarrow {}^6H_{5/2}$, and $^6P_{7/2} \leftarrow {}^6H_{5/2}$ $^6P_{5/2}$ for Sm^{3+}.[48] Under the excitation of 253 nm, the complex **3** shows three emission peaks at 561, 589 and 658, which may be attributed to $^4G_{5/2} \rightarrow {}^6H_{5/2}$, $^4G_{5/2} \rightarrow {}^6H_{7/2}$, $^4G_{5/2} \rightarrow {}^6H_{9/2}$ transitions respectively (Figure 7).

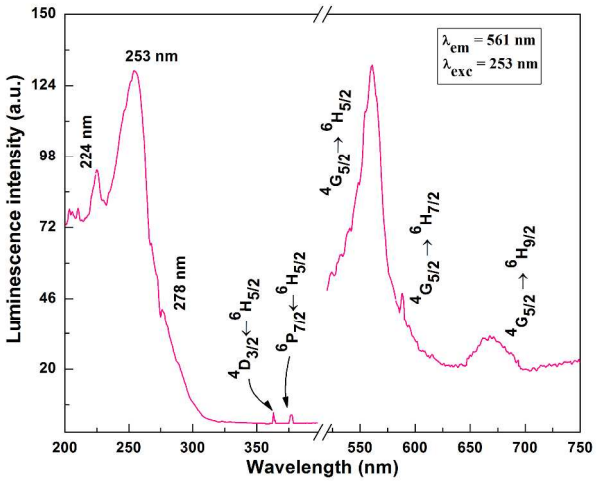

Figure 7 Excitation and emission spectra of [Sm(PDH)(ox)(H_2O)] **3** at λ_{em} = 561 nm, and λ_{exc} = 253nm respectively.

3.7. Life time and quantum yield measurements

The room temperature decay curve $^5D_0$ (Eu^{3+}) of complex **1** in solid state was monitored within the more intense peak of $^5D_0 \rightarrow {}^7F_2$ (617 nm) when excited at 282 nm. The emission decay curve (Fig. 8) is well fitted by a single-exponential function. The determined lifetime values of complex **1** is 0.321 ms. Generally the total quantum yield (Φ_{tot}) of ligand-sensitized lanthanide complex emission is the product of the ligand sensitization efficiency (η_{sens}) and the intrinsic quantum yield (Φ_{Ln}) of the lanthanide luminescence according to the following equation: [49]

$$\Phi_{tot} = \eta_{sens} \cdot \Phi_{Ln} \qquad (1)$$

The ligand energy transfer efficiency (η_{sens}) is the product of the two processes: intersystem crossing (ISC) from the ligand's first excited singlet level to the triplet energy level and energy transfer (LET) to the lanthanide. The intrinsic quantum yield of the lanthanide luminescence (Φ_{Ln}) can be judged on the basis of observed luminescence lifetime (τ_{obs}) and pure radiative lifetime

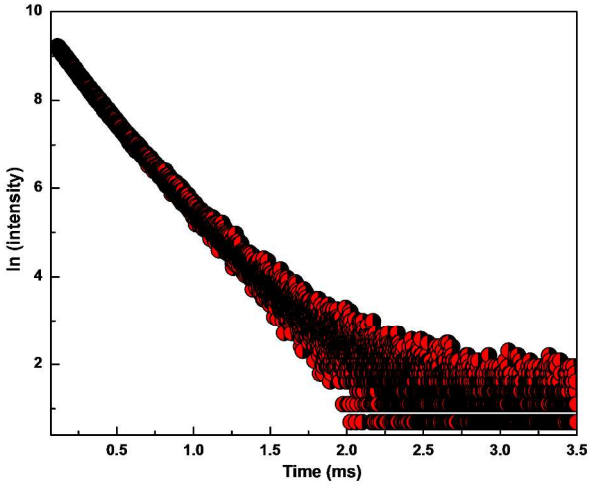

Figure 8 Emission decay curves of $^5D_0$ emitting state of complex **1**.

(τ_R) of the Eu(III) $^5D_0 \rightarrow {}^7F_J$ (J = 0–4) transitions by using following equation:[50]

$$\Phi_{Ln} = \tau_{obs}/\tau_R \qquad (2)$$

$$1/\tau_R = A_{MD,0}\, n^3 (I_{tot}/I_{MD}) \qquad (3)$$

where $A_{MD, 0}$ = 14.65 s^{-1} is the spontaneous emission probability of the $^5D_0 \rightarrow {}^7F_1$ transition of Eu^{3+}; n, the refractive index of the medium; $I_{tot}/I_{MD,0}$ the ratio of the integrated total area of the corrected Eu^{3+} emission spectrum to the area of magnetic dipole $^5D_0 \rightarrow {}^7F_1$ transition. According to equation (3), the radiative lifetimes (τ_R) can be calculated as 6.1 ms. Overall quantum yields (Φ_{tot}) was determined as 2.68%. Then on the basis of equations (2) and (3), the intrinsic quantum yields (Φ_{Ln}), sensitization efficiencies (η_{sens}) and the experimentally determined luminescence lifetimes (τ_{obs}) of complex **1** are 5.26%, 50.95% and 0.321 ms, respectively.

3.8 Thermal Analysis

The TG and DTA curves of the titled complexes **1** ~ **4** were performed as shown in Figure S7. The TGA/DTA curves for complexes **1** ~ **4** show that they undergo two major weight loss processes under 800 °C. The complexes can be stable up to 321.3 °C for complex **1**, up to 324.1 °C for complex **2**, up to 320.1°C for complex **3** and up to 321.5 °C for complex **4**. The first weight loss can be attributed to loss of one coordinated water molecule (calcd: 4.2 %, found 4.5 % for complex **1**; calcd: 4.2 %, found: 4.4 % for complex **2**; weight loss calc: 4.3 %, found: 4.7 for complex **3**; calcd: 4.2 %, found: 4.8% for complex **4**), which is in the endothermic DTA temperature range of 125.1~202.1 °C for complex **1**, 125.1~202.4 °C for complex **2**, 125.1~200.3 °C for complex **3**, and 125.1~170.4 °C for complex **4**, respectively. The second major weight loss can be attributed to the release of organic parts H_2PDH and oxalic acid (calcd: 21.0 %, found: 21.3 % for complex **1**; calcd: 20.6 %, found: 21.1 % for complex **2**; calcd: 21 %, found: 21.8 % for complex **3**, and calcd: 20.7 %, found: 21.5% for complex **4**), which is in the endothermic DTA temperature range of 321.3~743.2 °C for complex **1**, 324.1~744.8 °C for complex **2**, 320.1~742.8 °C for complex **3**, and 321.5~743.4 °C for complex **4**, respectively. The final residues of complexes **1** ~ **4** may be attributed as Ln_2O_3 (Ln = Eu, Tb, Sm and Gd).

3.8. Potential of complexes for sensing small molecules

The solvent molecules present in the first coordination sphere of the metal strongly influence the Ln^{3+} (Eu^{3+}, Sm^{3+} and Yb^{3+}) luminescence by ligand-to-metal charge transfer (LMCT) states.[51] In order to study the potential of titled complexes for sensing the solvent molecules, complex Eu(HPDH)(ox)(H_2O) **1** in which the energy transition from the triplet energy level ($^3\pi\pi^*$) of ligand $HPDH^-$ to Eu^{3+} cation is more effective was selected as a model for this study. The fine powder of complex **1** was added in eleven different solvents to get emulsion for photoluminescence study at room temperature. The photoluminescence (PL) is mainly dependent on the identity of solvent molecules.[52] The complex **1**–solvent emulsion was prepared by introducing 5 mg of complex **1** powder into 5.00 mL of 99.9% pure EtOH, MeOH, MeCN, $CHCl_3$, CH_2Cl_2, THF, $(C_2H_5)_2O$, H_2O, EtOAc, $(CH_3)_2O$ and DMF. Under same condition their PL emission behavior was

studied at excitation wave length of 282 nm, the PL emission spectra of all samples of complex **1** shows four typical Eu^{3+} cation's transitions as $^5D_0 \rightarrow {}^7F_n$ (n= 1, 2, 3, 4), among them $^5D_0 \rightarrow {}^7F_2$ transition (617 nm) has highest intensity, so the peak at 617 nm was selected as a reference for all further PL study (Figure S8). As shown in Figure 9, the PL intensity is heavily dependent on the individuality of the solvent molecule. Ether has a negligible effect on the luminescence intensity, whereas others exhibit varying degrees of enhancing or quenching effects. Interestingly, Figure 9 demonstrates that PL emission spectra selectively depend upon the nature of solvent molecule, especially for EtOH and DMF. EtOH has the strongest sensitizing and DMF has significant quenching influence on the luminescence intensity of complex **1**, which almost disappeared when complex **1** was immersed in pure DMF. Such solvent-dependent luminescence properties are very interesting and important for the selective sensing of EtOH or DMF solvent molecules.

In order to understand the sensibility of complex **1** with respect to solvents, THF was monitored as a reference solvent, because its luminescence intensity lies in the middle of eleven solvents. Complex **1** was dispersed in THF as a standard emulsion, different concentrations of EtOH and DMF were added into the standard emulsion, while keeping Eu^{3+} concentration constant. The photoluminescence spectra of emulsions were measured after days of aging and stirred vigorously before testing.

The EtOH concentration was gradually increased in standard emulsion to monitor its enhancing effect as shown in Figure 10a, the PL intensity of standard emulsion gradually increased with increasing the concentration of EtOH, which was nearly proportional to the EtOH concentration (Figure 10a inset). On the other hand, addition of DMF to standard emulsion led to significant quenching fluorescence intensity, which almost dismissed at and after 83.0 % (4.15 mg) (Figure 10b) and also the quenching intensity was nearly proportional to the DMF concentration (Figure 10b inset).

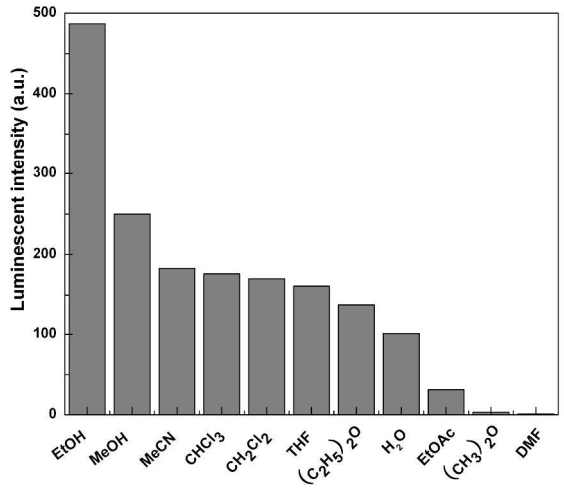

Figure 9 The $^5D_0 \rightarrow {}^7F_2$ transition intensities of complex **1** introduced into various pure solvents when excited at 282 nm.

The increasing and decreasing trend of the fluorescence intensity of Eu^{3+} at 617 nm ($^5D_0 \rightarrow {}^7F_2$) against the volume ratio of EtOH and DMF respectively, can be well fitted with a first-order exponential decay (PL intensity of standard emulsion as a function of EtOH and DMF), indicating that fluorescence quenching of complex **1** by DMF and fluorescence increasing of **1** are diffusion-controlled.

Furthermore the reusability of the complex **1** was also studied by taking EtOH, MeCN, $CHCl_3$ and THF as examples, the sensing ability of the complex **1** was explored by filtering off the dispersed solution, washing several times with EtOH and drying under vacuum at 323 K for 6 h. It is noteworthy that complex **1** almost regains its initial fluorescence intensity, implying a high photo stability of the material for a long time without any contamination (Figure S9).

In order to understand the general solvent pattern toward PL intensity of complex **1**, we divided the eleven solvents into four groups as; polar protic (EtOH, MeOH, H_2O), polar aprotic (MeCN, $CH_3)_2O$, DMF), non polar ($CHCl_3$, $(C_2H_5)_2O$) and border line polar aprotic (CH_2Cl_2, THF, EtOAc). It was observed that PL intensity of complex **1** is proportional and inversely proportional to the dielectric constant, coordination ability and Reichardt values (E_T^N) for polar aprotic, nonpolar solvents and polar protic solvents respectively, while in case of border line polar aprotic solvents PL intensity increases with increase of dielectric constant and Dimroth–Reichardt E_T parameter and decreases with the increase of coordination ability as listed in Table S1.[53-55] Although the mechanism for such enhancing and quenching effects of small solvent molecules is still not apparent, however the binding interaction of the lanthanide metal with small guest solvent molecules in the periphery of its first coordination sphere definitely play a major role.

DMF has a different effect on the photoluminescence intensity due to its high coordination ability with Eu^{3+} which is known as solvent effect. The present ligand (H_2PDH) containing O and N donor sets forms a caved conformation suitable for the coordination with lanthanide ions, but this ajar cavity could not prevent absolutely the solvent molecules from entering.

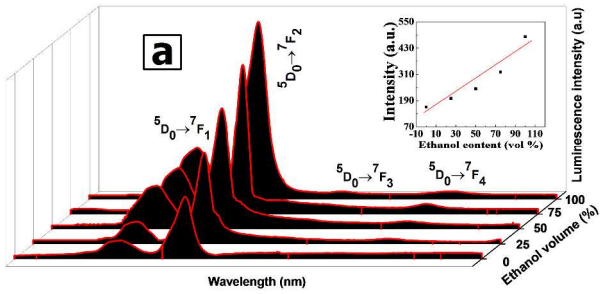

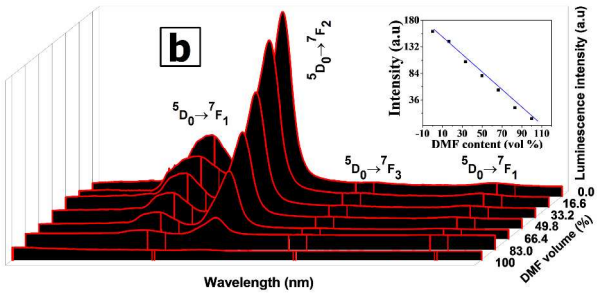

Figure 10 The Photoluminescence spectra of complex **1**-THF emulsion in the presence of various content of ethanol (a) and DMF (b), when excited at 282 nm.

Together with the raising coordination abilities of CH_3OH, CH_3CN, C_2H_5OH, THF for the lanthanide ions in this system, the oscillatory motions of the entering molecules consume more energy which the ligand triple level transfer to the emitting level of the lanthanide ion.[56] As a result, the entering solvent will consume more energy of the triplet state energy of ligand transferring to the resonant energy level of the Eu^{3+}. It is likely to expect that the weakly coordinated THF molecules with Eu^{3+} sites are slowly replaced by EtOH and DMF molecules, leading to their luminescence enhancement and quenching, respectively.

4. Conclusion

Four 3-D supramolecular frameworks constructed from 2-D coordinated layers have been synthesized by using two ligands (oxalic acid and 6,7-dihydropyrido(2,3-*d*)pyridazine-5,8-dione). Single crystal X-ray diffraction analysis revealed that the different coordination modes of the organic ligand could promote the formation of versatile 2-D coordination layers. Eu^{3+} and Tb^{3+} complexes showed high photoluminescent intensity, followed by Sm^{3+} complex, as the triplet energy level of H_2PDH and oxalic acid ligands lie close to the resonating energy levels of Eu^{3+} and Tb^{3+} respectively. The sensing potential of Eu^{3+} complex **1** for small molecules revealed that it can be used as sensing probe for ethanol and DMF, as ethanol was found to be an excellent sensitizer solvent while DMF as highly quenching solvent. Photoluminescence intensity of complex **1** decreases with the increase of dielectric constant, coordination ability and Dimroth–Reichardt E_T parameter (E_T^N) values for polar protic solvents, while increases with the increase of dielectric constant, Dimroth–Reichardt E_T values and coordination ability values for polar aprotic and nonpolar solvents. The complex **1** excellently regained its first photoluminescent intensity, revealing an interesting prospect for its long-term reusability. Our new finding contribute to molecular sensing with porous lanthanide-organic coordination polymers, provide useful information about the design of stable, and sensitive lanthanide-organic coordination polymers for sensing small guest molecules in the future. In addition the available coordination sites and pores in these lanthanide-organic coordination polymers may be used for post synthetic covalent modification for further application, efforts to realize these are underway.

Acknowledgement

The financial support from the National Natural Science Foundation of China (No. 20975009) is greatly acknowledged.

Notes and references

[a] *State Key Laboratory of Chemical Resource Engineering, Institute of Science, Beijing University of Chemical Technology, Beijing 100029, P. R. China.*

†Electronic Supplementary Information (ESI) available: Synthetic scheme of ligand H_2PDH, ^{1}HNMR of ligand, IR spectra of ligand and complexes **1** ~ **4**, powder X-ray diffraction patterns of complexes **1** ~ **4**, weak forces interaction in complex **1**, UV spectrum of free H_2PDH ligand, phosphorescence spectrum of [Gd(HPDH)(ox)(H_2O)] **4**, TG and DTA curves of complexes **1** ~ **4**, PL spectra of complex **1**-solevent emulsions in different solvents and reproduce ability of complex **1**, and dielectric constant, coordination ability and Reichardt E_T parameters. For ESI and crystallographic data in CIF or other electronic format see DOI: 10.1039/b000000x/

(1) (a) Lakowicz, J. R. *Topics in Fluorescence Spectroscopy*, vol. 2, Principles, Plenum Press, New York, 1991. (b) L. –G. Qiu, Z. –Q. Li, Y. Wu, W. Wang, T. Xu and Xia. Jiang, *Chem. Commun*., 2008, 3642.

(2) Lakowicz, J. R., Topics in Fluorescence Spectroscopy. Vol.1, Techniques. Lakowicz, Joseph R. Publication: Kluwer Academic Publishers, New York 2002.

(3) W. Yang, J. Feng and H. Zhang, *J. Mater. Chem.,* 2012, **22**, 6819.

(4) B. Chen, Y. Yang, F. Zapata, G. Lin, G. Qian and E. B. Lobkovsky, *Adv. Mater.,* 2007, **19**, 1693.

(5) D. Ma, W. Wang, Y. Li, J. Li, C. Daiguebonne, G. Calvez and O. Guillou, *CrystEngComm.,* 2010, **12**, 372.

(6) H. -L. Jiang, Y. Tatsu, Z. -H. Lu and Q. Xu, *J. Am. Chem. Soc*. 2010, **132**, 5586.

(7) Y. Cui, Y. Yue, G. Qian and B. Chen, *Chem. Rev*., 2012, **112**, 1126.

(8) (a) R. Matsuda, R. Kitaura, S. Kitagawa, Y. Kubota, T. C. Kobayashi, S. Horike and M. Takata, *J. Am. Chem. Soc*., 2004, **126**, 14063; (b) T. K. Maji, K. Uemura, H. -C. Chang, R. Matsuda and S. Kitagawa, *Angew. Chem., Int. Ed.,* 2004, **43**, 3269; (c) C. Serre, F. Millange, C. Thouvenot, M. Nogues, G. Marsolier, D. Louer and G. Ferey, *J. Am. Chem. Soc.,* 2002, **124**, 13519.

(9) (a) K. Biradha, Y. Hongo and M. Fujita, *Angew. Chem., Int. Ed.,* 2002, **41**, 3392; (b) G. J. Halder, C. J. Kepert, B. Moubaraki, K. S. Murray and J. D. Cashion, *Science*. 2002, **298**, 1762; (c) T. K. Maji, G. Mostafa, R. Matsuda and S. Kitagawa, *J. Am. Chem. Soc.,* 2005, **127**, 17152; (d) A. Kondo, N. Hiroshi, L. Carlucci, D. M. Proserpio, G. Ciani, H. Kajiro, T. Ohba, H. Kanoh and K. Kaneko, *J. Am. Chem. Soc.,* 2007, **129**, 12362.

(10) (a) K. Takaoka, M. Kawano, M. Tominaga and M. Fujita, *Angew. Chem., Int. Ed.,* 2005, **44**, 2151; (b) D. N. Dybtsev, H. Chun and K. Kim, *Angew. Chem., Int. Ed.,* 2004, **43**, 5033; (c) C. Serre, C. Mellot-Draznieks, S. Surble, N. Audebrand, Y. Filinchuk and G. Ferey, *Science.,* 2007, **315**, 1828; (d) E. J. Cussen, J. B. Claridge, M. J. Rosseinsky and C. J. Kepert, *J. Am. Chem. Soc.,* 2002, **124**, 9574; (e) M. P. Suh, J. W. Ko and H. J. Choi, *J. Am. Chem. Soc.,* 2002, **124**, 10976; (f) K. Uemura, Y. Yamasaki, Y. Komagawa, K. Tanaka and H. Kita, *Angew. Chem., Int. Ed.* 2007, **46**, 6662.

(11) K. Biradha, Y. Hongo and M. Fujita, *Angew. Chem. Int. Ed*. 2002, **41**, 3395.

(12) P. Amo-Ochoa, P. J. S. Miguel, O. Castillo and F. Zamora, *CrystEngComm.,* 2007, **9**, 987.

(13) X. -H. Jin, J. -K. Sun, L. -X. Cai and J. Zhang, *Chem. Commun.,* 2011, **47**, 2667.

(14) K. L. Gurunatha and T. K. Maji, *Inorg. Chem.,* 2009, **48**, 10886.

(15) Y. Bai, G. -J. He, Y. -G. Zhao, C. -Y. Duan, D. -B. Dang and Q. -J. Meng, *Chem. Commun.,* 2006, 1530.

(16) J. Jin, F. -Q. Bai, G. -H. Li, M. -J. Jia, J. -J. Zhao, H. -L. Jia, J. -H. Yu and J. -Q. Xu, *CrystEngComm*., 2012, **14**, 8162.

(17) A. G. Talma, P. Jouin, J. G. D. Vries, C. B. Troostwijk, G. H. W. Buning, J. K. Waninge, J. Visscher and R. M. Kellogg, *J. Am. Chem. Soc.,* 1985, **107**, 3981.

(18) J. Jin, D. Wu, M. -J. Jia, Y. Peng, J. -H. Yu, Y. -C. Wang and J. -Q. Xu, *J. Solid State Chem.,* 2011, **184**, 667.
(19) (a) G. M. Sheldrick, SHELXTL V5.1, Software Reference Manual, Bruker AXS, Inc, Madison, WI, 1997; (b) W. S. Sheldrick and M. Morr, *Acta. Crystallogr., Sect. B.,* 1981, **37**, 733.
(20) (a) G. M. Sheldrick, SHELXTL-97, a Program for Crystal Structure Refinement, University of Göttingen, Germany, 1997; (b) G. M. Sheldrick, SHELXS97, Program for Crystal StructureSolution; University of Gottingen: Gottingen, Germany, 1997.
(21) J. A. Kaizerman, W. Aaron, S. An, R. Austin, M. Brown, A. Chong, T. Huang, R. Hungate, B. Jiang, M. G. Johnson, G. Lee, B. S. Lucas, J. Orf, M. Rong, M. M. Toteva, D. Wickramasinghe, G. Xu, Q. Ye, W. Zhong and D. L. McMinn, *Bioorg Med Chem Lett*., 2010, **20**, 4607.
(22) I. A. Jankovic, Z. V. Saponjic, E. S. Dzunuzovic and J. M. Nedeljkovic, *Nanoscale Res. Lett.,* 2009, **5**, 81.
(23) P. Chawla, R. Maheshwari, S. A. Saraf*., Der. Pharma. Chemica*. 2010, **2**, 38.
(24) A. Sengul and H. Arslan, *Turk. J. Chem.* 2008, **32**, 355.
(25) J. J. Ding, H. F. Jiu, J. Bao, C. J. Lu, W. R. Gui, Q. J. Zhang, C. Gao, *J. Comb. Chem*. 2005, **7**, 69.
(26) S. Sato and M. Wada, *Bull. Chem. Soc. Jpn*. 1970, **43**, 1955.
(27) S. L. Wu, Y. L. Wu and Y. S. Yang, *J. Alloys Compd.,* 1992, **180**, 399.
(28) D. L. Dexter, *J. Chem. Phys.,* 1953, **21**, 836.
(29) G. A. Crosby, R. M. Alire*., J. Chem. Phys*. 1961, **34**, 743.
(30) F. J. Steemers, W. Verboom, D. N. Reinhoudt, E. B. van der. Tol and J. W. Verhoeven, *J. Am. Chem. Soc.,* 1995, **117**, 9408.
(31) (a) M. D. Regulacio, M. H. Pabilco, J. A. Vasquez, P. N. Myers, S. Gentry, M. Prushan, S. -W. Tamchang, S. L. Stoll, *Inorg. Chem.,* 2008, **47**, 1512; (b) R. D. Archer, H. Y. Chen, L. C. Thompson, *Inorg. Chem.,* 1998, **37**, 2089.
(32) S. Biju, D. B. Ambili Raj, M. L. P. Reddy and B. M. Kariuki, *Inorg. Chem*. 2006, **45**, 10651.
(33) (a) L. Armelao, S. Quici, F. Barigelletti, G. Accorsi, G. Bottaro, M. Cavazzini, E. Tondello, *Coord. Chem. Rev.,* 2010, **254**, 487; (b) W. T. Carnall, P. R. Fields and K. Rajnak, *J. Chem. Phys.,* 1968, **49**, 4443.
(34) P. Wang, R. -Q. Fan, X. -R. Liu, L. -Y. Wang, Y. -L. Yang, W. -W. Cao, B. Yang, W. Hasi, Q. Su and Y. Mu, *CrystEngComm*., 2013, **15**, 1931.
(35) M. Latva; H. Takalo; V. M. Mukkala, C. Matachescu, J. C. Rodriguez-Ubis, J. Kankare, *J. Lumin.,* 1997, **75**, 149.
(36) M. V. Lucky, S. Sivakumar, M. L. P. Reddy, A. K. Paul and S. Natarajan, *Cryst. Growth Des*. 2011, **11**, 857.
(37) Y. -L. Jiang, Y. -L. Wang, J. -X. Lin, Q. -Y. Liu, J. –J. -Wei, Z. -H. Lu, N. Zhang and L. -Q. Li, *CrystEngComm*., 2011, **13**, 1697.
(38) C. -H. Liang, Y. -C. Chang, Y. -S. Chang, *Appl. Phys. Lett*. 2008, **93**, 211902.
(39) P. C. R. Soares-Santos, L. Cunha-Silva, F. A. A. Paz, R. A. S. Ferreira, J. Rocha, L. D. Carlos, H. I. S. Nogueira, *Inorg. Chem.,* 2010, **49**, 3428.
(40) (a) Y. F. Yuan, T. Cardinaels, K. Lunstroot, K. V. Hecke, L. V. Meervelt, C. Gorller-Walrand, K. Binnemans and P. Nockemann, *Inorg. Chem*. 2007, **46**, 5302; (b) D. Weng, X. Zheng, X. Chen, L. Li, L. Jin, *Eur. J. Inorg. Chem.,* 2007, 3410.
(41) B. Francis, D. B. Ambili Raj and M. L. P. Reddy, *Dalton Trans.,* 2010, **39**, 8084.
(42) D. B. Raj, B. Francis, M. L. P. Reddy, R. R. Butorac, V. M. Lynch and A. H. Cowley, *Inorg. Chem.,* 2010, **49**, 9055.
(43) A. F. Kirby, D. Foster and F. S. Richardson, *Chem. Phys. Lett.,* 1983, **95**, 507.
(44) G. R. Choppin and D. R. Peterman, *Coord. Chem. Rev.,* 1998, **174**, 283.
(45) Y. G. Sun, X. M. Yan, F. Ding, E. J. Gao, W. Z. Zhang and F. Verpoort, *Inorg. Chem. Commun.,* 2008, **11**, 1117.
(46) Z. Zhang, J. Yuan, X. Wang, D. Xiong, H. Chen, J. Zhao, Y. Fu, Z. Qi, G. Zhang, C. Shi, *J. Phys. D: Appl. Phys.,* 2007, **40**, 1910.
(47) U. Caldino, A. Speghini and M. Bettinelli, *J. Phys. Condens. Mater.,* 2006, **18**, 3499.
(48) Y. -Q. Sun, J. Zhang and G. -Y. Yang, *Chem. Commun.,* 2006, 1947.
(49) (a) M. Xiao and P. R. Selvin, *J. Am. Chem. Soc*., 2001, **123**, 7067; (b) S. Comby, D. Imbert, A. Chauvin, J. G. Bunzli, L. J. Charbonniere and R. F. Ziessel, *Inorg. Chem*., 2004, **43**, 7369.
(50) M. H. V. Werts, R. T. F. Jukes and J. W. Verhoeven, *Phys. Chem. Chem.Phys*., 2002, **4**, 1542.
(51) (a) G. F. de Sa, O. L. Malta, C. D. Donega, A. M. Simas, R. L. Longa, P. A. Santa-Cruz and E. F. da Silva, *Coord. Chem. Rev.,* 2000, **196**, 165; (b) F. R. Concalves e Silva, O. L. Malta, C. Reinhard, H. U. Gudel, C. Piguet, J. E. Moser and J. -C. G. Bunzli, *J. Phys. Chem. A.,* 2002, **106**, 1670; (c) F. R. Concalves e Silva, R. L. Longo, O. L. Malta, C. Piguet and J. -C. G. Bunzli, *Phys. Chem. Chem. Phys.,* 2000, **2**, 5400.
(52) D. Ma, W. Wang, Y. Li, J. Li, C. Daiguebonne, G. Calvez and O. Guillou, *CrystEngComm.,* 2010, **12**, 4372.
(53) J. A. Riddick, W. B. Bunger, T. K. Sakano, Organic solvents: physical properties and methods of purification. **1986** Fourth edition, John Wiley and Sons,New York, NY.
(54) D. T. Raul and A. Santiago, *Dalton Trans.,* 2011, **40**, 10742.
(55) R. Christian, *Chem. Rev*. 1994, **94**, 2319.
(56) F. Dang, W. Liu, J. Zheng, *J. Fluoresc.,* 2007, **17**, 89.

Graphical abstract

The 2-D lanthanide-organic complex $[EuHPDH)(ox)(H_2O)]_n$, synthesized under hydrothermal condition, shows high potential for sensing the small molecules by its luminescence properties in different emulsions.